*Int. J. Electrochem. Sci.*, 10 **(2015)** 6359 - 6377

International Journal of
ELECTROCHEMICAL
SCIENCE
www.electrochemsci.org

# Oxidation Behaviour of Laser Welding of TP347HFG and VM12-SHC Stainless Steels

*Mieczyslaw Scendo*[1,*], *Milena Chat*[1], *Bogdan Antoszewski*[2]

[1] Institute of Chemistry, Jan Kochanowski University in Kielce, Swietokrzyska 15G, PL- 25406 Kielce, Poland
[2] Centre for Laser Technologies of Metals, University of Technology in Kielce, 1000-lecia Panstwa Polskiego 7, PL-25314 Kielce, Poland
[*]E-mail: scendo@ujk.edu.pl

*Received:* 30 April 2015 / *Accepted:* 25 May 2015 / *Published:* 24 June 2015

The oxidation behaviour of laser welded of TP347HFG and VM12-SHC stainless steels in air atmosphere were investigated. The temperature was changed from 25 to 1400 $^0$C. The stainless steels butt were welded. Materials were examined by the thermogravimetric method. The surface and microstructure of the sample were observed in an optical microscope (OM) and a scanning electron microscope (SEM). The X-ray fluorescence spectrometer (XRF) was used to observation change in chemical composition along the cross-section of specimen. The results showed the substantial intermixing of both substrates within the fusion zone. The thermogravimetric data indicate that the investigated materials undergo chemical corrosion. The thermodynamic parameters formation oxides on substrates were calculated and discussed. The $CO_2$ laser welding technique was suggested as a good method for joining dissimilar steels.

**Keywords:** Laser welding; Joint, Austenitic, Martensitic, Thermogravimetric analysis, Activation energy

## 1. INTRODUCTION

The consumer industry has been incorporating a variety of materials in its products made on a large scale to improve performance and reduce costs. It results in increased demands for techniques concerning weld dissimilar materials and for using industrial production on a large scale [1-3].

Stainless steels are alloys which are widely applied in various industrial sectors such as marine, chemical, desalination and petrochemical industries. They are commonly used for fabricating engineering components including immersion water heaters and novel thermal sensors owing to their

good weldability, high corrosion resistance and mechanical strength [4]. Mechanical properties of other steels can be changed by heat treatment. Austenitic and martensitic stainless steels are most widely used to produce modern energetistic devices [5]. These steels are usually used for a wide range of applications such as steam generators, pressure vessels, mixer blades, cutting tools and off-shore platforms for oil extraction [6]. The joining of dissimilar materials is one of the most challenging tasks facing modern manufactures. Dissimilar metal joints are widely used in various industrial applications for both technical and economic reasons. Austenitic and martensitic stainless steels with their chromium and carbon contents are resistant to various environmental conditions. Moreover, nickel and molybdenum content provides the elevated-temperature strength through the formation of stable carbide both metals [7]. Austenitic stainless steel can be very easily welded with traditional welding processes like *arc* welding. Only martensitic stainless steel with high carbon can have cracking problems like hydrogen induced cracking. The weldability of dissimilar metals is determined by their atomic diameter, crystal structure and compositional solubility in liquid or solid states. The laser welding technique was suggested as a modern method of joining two metals of different properties. Laser welding is a high energy density process and well-known for its deep penetration, high speed, small heat-affected zone, fine welding seam quality, low heat input per unit volume [8]. A butt joint is one of the most common laser welded materials used to produce tubes and tailor welded blanks [9-12]. The material being welded must be clean. It is of profit to all welding, but even more important to laser welding. Unfortunately, in the case of dissimilar materials the butt joint is subject to chemical and electrochemical corrosion at the high temperature or in an aggressive environment, particularly in the presence of chloride ions [13].

Numerous thermal analysis techniques are available for quantitative and qualitative studies on the thermal behaviour of materials in the laboratory. Among them, the thermogravimetric analysis offers advantages of good control over the temperature and heating rate as well as the rapid and reliable comparison of thermal decomposition processes of materials of different chemical constituency when few details on reactions or products are available [14-16].

The present paper concerns oxidation resistance laser welded joint of TP347HFG (austenitic) and VM12-SHC (martensitic) stainless steels. The samples were examined using a thermogravimetric analyzer (TGA) in air atmosphere. The surface and microstructures were observed by an optical microscope (OM) and a scanning electron microscope (SEM). The X-ray fluorescence spectrometer (XRF) was used to determine variations of the main chemical elements across the fillet weld.

## 2. EXPERIMENTAL

### *2.1. Materials*

The materials of TP347HFG and of VM12-SHC stainless steels were designed for the laser welding. Table 1 presents the chemical composition of both steels.

**Table 1.** Chemical composition of stainless steels

| Steel wt% | C | S | Si | Mn | Mo | Co | W | P | Cr | Ni | V | Nb |
|---|---|---|---|---|---|---|---|---|---|---|---|---|
| TP347HFG | 0.08 | 0.03 | 0.75 | 2.00 | - | - | - | 0.04 | 18 | 9 | - | 0.64 |
| VM12-SHC | 0.12 | - | 0.50 | 0.30 | 0.30 | 1.60 | 1.50 | - | 12 | - | 0.25 | 0.05 |

*The TP347HFG or VM12-SHC stainless steels contain of 69.46 or 83.38% Fe respectively.*

Samples for welding were prepared by cutting pipes to size 150 mm from base materials. The diameter of pipes was 80 mm and the wall thickness was 5 mm.

### *2.2. $CO_2$ laser welding system*

The carbon dioxide ($CO_2$) laser (**l**ight **a**pplication by the **s**timulated **e**mission of **r**adiation) is the most powerful type of industrial laser available now. It is generally used for contour cutting and deep penetration welding. The long wavelength of $CO_2$ light 10.6 μm is absorbed by most solids. This allows $CO_2$ lasers to process a wide variety of materials. The $CO_2$ laser welding system was used for the melting of two stainless steels. The TRUMPF LASERCELL 1005 (TLC 1005) with 6 kW power made it possible to produce short and long series of different materials at low costs and in a short time. The bifocal welding head was used for the joining of steels. The focal length averaged out at 200 mm, and the span at 0.7±0.05 mm. The focus were ranged in order one by second in welding direction. The welding velocity was 160 mm/min in *X*-direction for the trial tests to perform a successful welding. The laser beam was positioned at the joint (and moved) 2 mm in relation to the surface of a sample. Helium gas at the pressure of 200 Pa and speed of 18 L/min was used as the shield gas which protected the heated surface from oxidation.

### *2.3. Laser welded joint*

The schematic diagram of the laser welded joint is shown in Figure 1. The materials in the form of pipes were butt welded. The full joint penetration was applied. The joint was initially examined in an optical microscope.

The cross-section of the weld fillet was observed to determine the geometry, depth of penetration and cracks in the heat-affected zone (HAZ) as well as in the welded zone (WZ) of the joint. The geometry and cross-sectional dimensions of the weld helped define its average area. Moreover, no special heat treatment was carried out after laser welding.

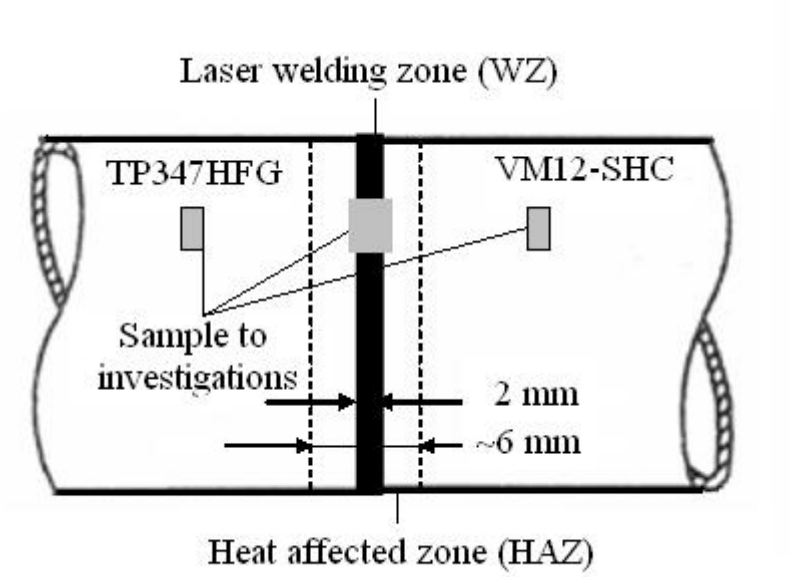


**Figure 1.** Schematic diagram of laser welded joint of TP347HFG and VM12-SHC stainless steels

*2.4. Thermogravimetric measurements*

Thermogravimetric measurements were carried out on an NETZSCH STA Jupiter 449 thermogravimetric analyzer (TGA). Samples were prepared in the furnace of a thermobalance under controlled temperature to obtain the corresponding thermogravimetry (TG). The TG baselines were corrected by subtraction of predetermined baselines which are determined under identical conditions except for the absence of a sample. The sample in the furnace was heated up from 25 to 1400 $^0$C with the heating rate of 5 $^0$C min$^{-1}$. In order to eliminate the effects caused by the mass and heat transfer limitations, small quantities of samples (around 600 mg) were put into a $Al_2O_3$ crucible for each run under non-isothermal conditions. In addition, the oxidizing atmosphere inside the furnace of a thermogravimetric analyzer during temperature–programmed measurements was provided by means of a continuous airflow of 70 cm$^3$ min$^{-1}$. A thermogravimetric analyzer was applied for the thermal analysis of TP347HFG or VM12-SHC stainless steels, and the joint of both steels. The geometric surface area of the sample was 1.12 cm$^2$. Before every measurement each specimen was carefully polished with emery 2500 grade paper. Then, the sample was rinsed with double distilled water, degreased with ethanol and was immediately immersed in the furnace of a thermobalance.

*2.5. Thermogravimetry curve analysis*

Kinetic studies, based on the change of mass were obtained by the TG curve analysis [17-23]. The oxidation rate of materials at the high temperature can be estimated by the increase in scale thickness ($X_{scale}$), with time:

$$\beta_{scale} = \frac{d X_{scale}}{d t} \quad (1)$$

and this rate can also be expressed in terms of the mass gain:

$$k = \frac{\Delta m}{A\ t} \quad (1a)$$

where $\Delta m$ is the change mass of sample, $A$ is the surface area of the test specimen, and $t$ is the time of measurement. The oxidation rate of material was expressed as mg $cm^{-2}$ $h^{-1}$.

The activation energy for the oxidation process was calculated on basis the Arrhenius type plot according to the equation:

$$k = A\,exp\left(-\frac{E_a}{RT}\right) \quad (2)$$

or:

$$E_a = -RT\ ln\left(\frac{k}{A}\right) \quad (2a)$$

where $A$ is the Arrhenius pre-exponential constant, $E_a$ is the activation energy, $R$ is the universal gas constant, and $T$ is the absolute temperature. However, in the coordinate system of ln $k$ vs. $1/T$ a straight line whose slope allows an evaluation of the activation energy was obtained.

### *2.6. Additional measuring instruments*

The cross-section of the surface and microstructure of a sample was observed in an optical microscope (OM) and a scanning electron microscope (SEM), Joel, type JSM-5400. The accelerating voltage was 20 kV.

An X-ray fluorescence spectrometer (XRF) Thermo SCIENTIFIC type Niton XL3t was used to determine variations of the main chemical elements, in wt% (Fe, Cr and Ni) across the fillet weld at a depth of approximately 0.3 mm.

To evaluate the mechanical properties microhardness values were determined along the cross-section by the Vickers (HV) method using a Microtech MX3 tester under of 0.4 N load at a depth of 0.3 mm and at 0.07 mm intervals. This parameter was measured in the weld fillet and in the HAZ range.

Each test was repeated three times to verify the reproducibility of data and the average values were reported.

## 3. RESULTS AND DISCUSION

### *3.1. Laser welded joint*

The materials of TP347HFG (austenitic) and VM12-SHC (martensitic) stainless steels were butt welded. The Figure 2A shows that the cross-section of the joint had funnel-shaped appearance.

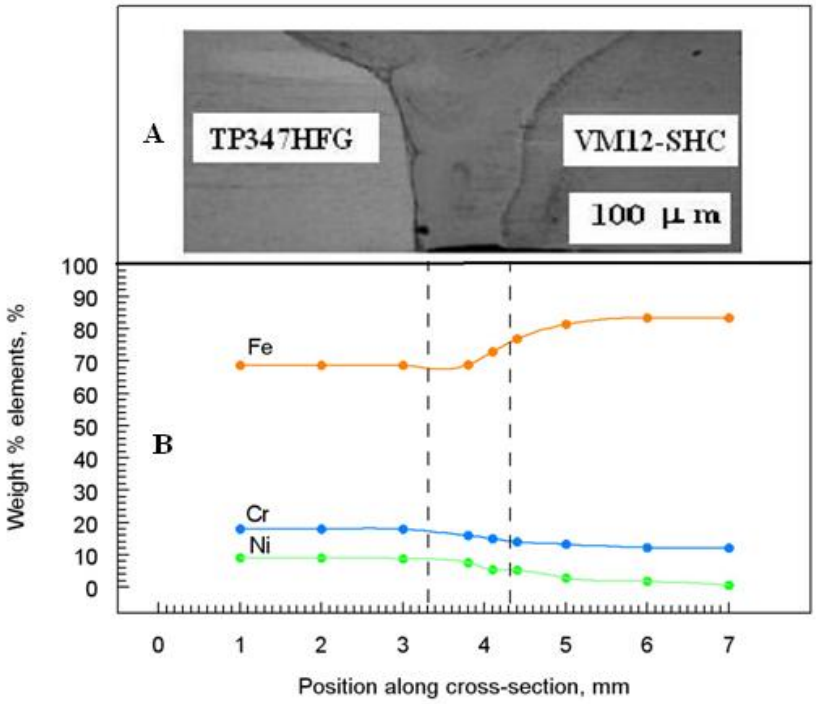


**Figure 2.** A- optical micrograph of joint penetration. Magnification 20×. B- change in chemical composition along the cross-section of specimen

The average width of the laser welding zone (WZ) at the weld sample face was 5 mm wide and 2 mm wide at the root. The width of the heat-affected zone (HAZ) was small in comparison to the welding electric arch. The average width of HAZ was 6 mm (Fig. 1). The laser welding surface was smooth without any spatter. Cracks were observed in the weld zone and in the heat-affected zone. Pores formed by the keyhole collapse during the welding were also not visible in the cross-section that were examined. The wt% of the main chemical elements in the fillet cross-section was obtained by energy dispersive spectroscopy. The graphs in Figure 2B show the wt% distribution of Fe, Cr and Ni along the weld cross-section. It can be observed that the chemical composition of the joint is different in comparison to that of both steels. The welding carried out the mixing components of TP347HFG and VM12-SHC stainless steels. It can be seen that in the weld zone the contents of iron increased but the concentrations of chrome and nickel decreased. Therefore, it seems that during the welding of austenitic and martensitic stainless steels the good mixing of the microstructure and components of both materials occurred.

### *3.2. Thermogravimetric measurements*

The change mass of materials in referring to time of exposition in air atmosphere and high temperature conditions, and thermogravimetry curves for TP347HFG, VM12-SHC stainless steels and joint are presented in Figure 3.

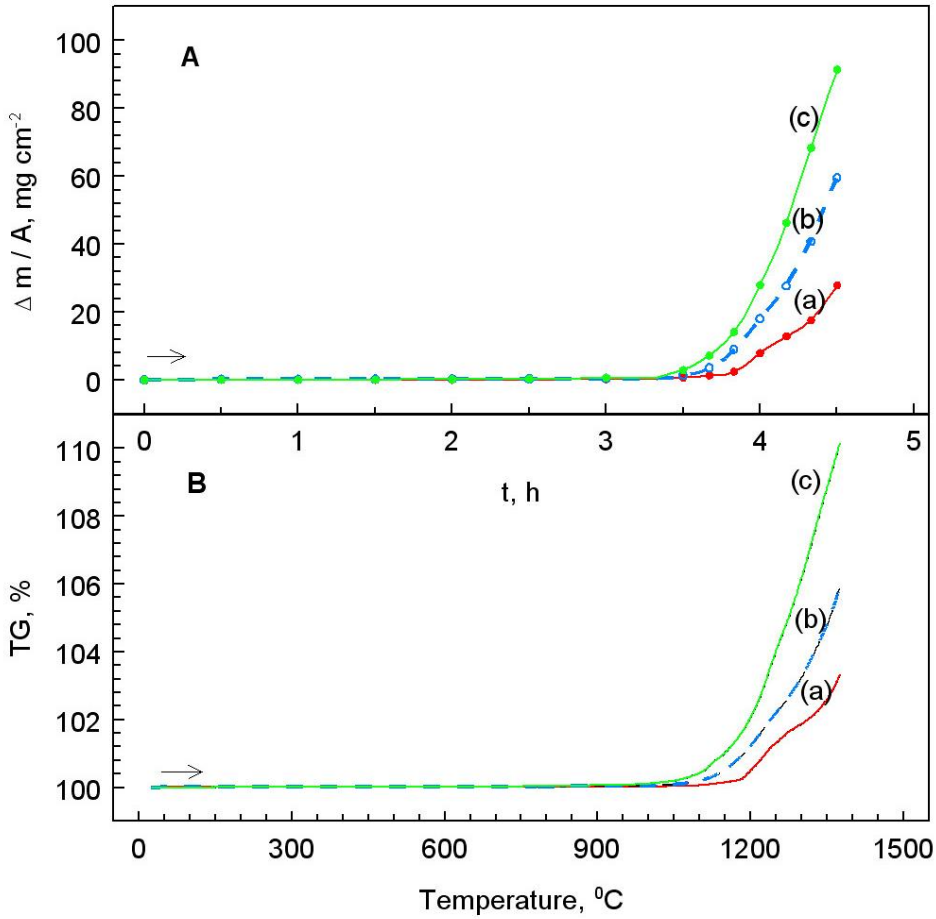


**Figure 3.** A – Change mass of materials in referring to time of exposition. B - Thermogravimetry curves. The samples: (a) TP347HFG, (b) joint and (c) VM12-SHC. Heating rate of 5 $^0$C min $^{-1}$

The weight gain of samples were observed after the achievement of the critical temperature conversion in which the increase of the mass of a sample achieved the value of 0.1% in relation to the mass of the initial specimen, Table 2.

**Table 2.** Materials, critical temperature conversion, weight gain of samples

| **Material** | **Critical temperature conversion $^0$C** | **Weight gain sample mg** |
|---|---|---|
| TP347HFG | 1145 | 20.01 |
| Joint | 1101 | 41.71 |
| VM12-SHC | 1049 | 62.69 |

However, in air atmosphere and high temperature the TP347HFG was the most resistant for oxidation in comparison to VM12-SHC stainless steel (Fig. 3). Moreover, the critical temperature conversion for the joint one was placed between both of stainless steels (see Table 2). However in Table 2 were listed the weight gain of samples after measurement. The largest increase of mass was registered for VM12-SHC but the smallest for TP347HFG stainless steel. However, in the case of joint a medium increase the mass was observed. Figure 4 show scanning electron microscope images internally oxidized of TP347HFG, joint and VM12-SHC stainless steel for 5 minutes at 1200 $^0$C in air atmosphere. The oxide layers can be observed near in the surface of specimens. The thickness of these oxide layers were measured. From these results, it is concluded that the thickness oxide layer for joint is the average value in reference to thickness oxide layers both steels. The oxidation mechanism of steel in air atmosphere and high temperature can depend on (i) the transport of oxidant gas from the bulk gas phase, (ii) phase boundary reaction(s) at the gas/scale interface, or (iii) the diffusion of iron cations to the scale/gas phase interface.

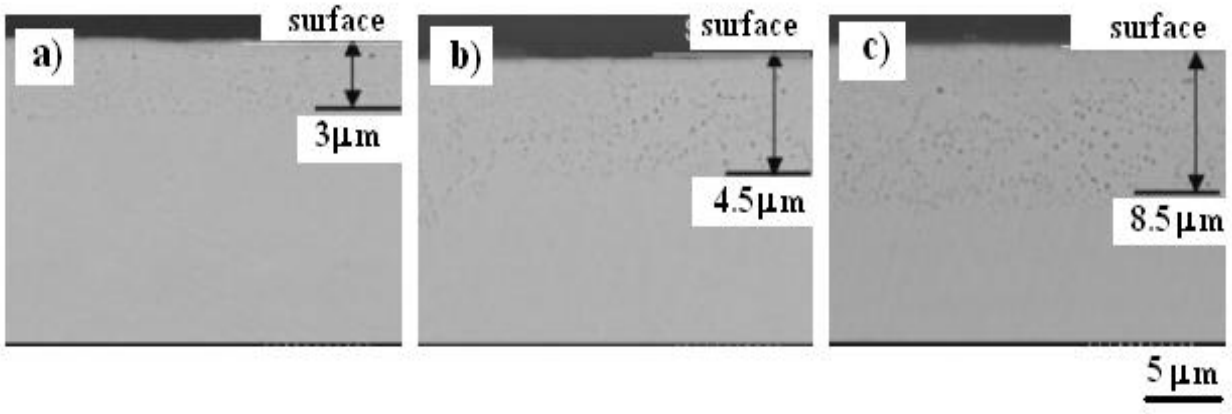


**Figure 4.** Scanning electron microscope images internally oxidized specimens for 5 minutes at 1200 $^0$C in air atmosphere: a) TP347HFG, b) joint and c) VM12-SHC

The oxidation of metal at the high temperature conditions can be considered as electrochemical process. In this case surface of the metal performs the part of anode. Then layer of oxides carries out the part as specific solid electrolyte. The outside surface of oxide layer performs the role of cathode. Therefore, the process of forming an oxide layer on the surface of the clean metal begins from the adsorption of oxygen:

Anode: $3\,Fe + 2\,O_{2\,(g)} \rightarrow Fe_3O_{4(S)}$ (3)

Cathode: $O_{2(g)} + 4\,e^- \rightarrow 2\,O^{2-}$ (3a)

and:

$2\,Fe_3O_{4(S)} + O^{2-} - 2\,e^- \rightarrow 3\,Fe_2O_{3\,(S)}$. (4)

The products of the iron oxidation of *magnetite* (reaction (3)) and *hematite* (reaction (4)) at the high temperature have a stratified structure. The spatial structure of layers of oxide is of ion character. The process of forming a layer of oxide on the metal depends on the diffusion of $Fe^{2+}$ through the layer in the direction of the gas phase (*from pithy diffusion*). Moreover, the diffusion ions of oxide from the

layer in the direction of the metallic basis (*to pithy diffusion*) is also possible [24]. The tight and suitable thick of the oxide layer should effectively protect the metal against the significant progress of the oxidation process. The mechanism oxidation of steel at the high temperature conditions was presented in Figure 5.

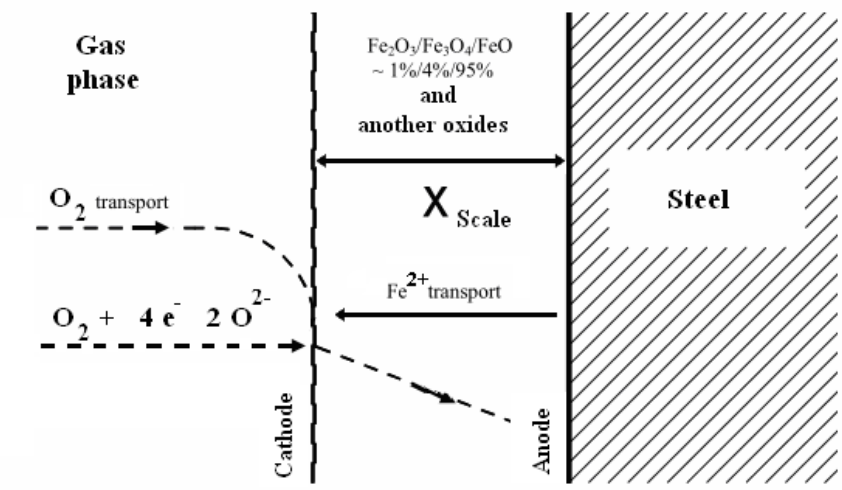


**Figure 5.** Mechanism oxidation of steel in air atmosphere and at the high temperature conditions

However, at temperature of 570 $^0$C causes the formation of the oxide layer (*scale*) according to the equations:

$$Fe^{2+} + Fe_3O_{4\,(S)} + 2\,e^- \leftrightarrow 4\,FeO_{(S)} \quad (5)$$

$$Fe^{2+} + 4\,Fe_2O_{3(S)} + 2e^- \leftrightarrow 3\,Fe_3O_{4(S)} \quad (5a)$$

furthermore:

$$2\,Fe_3O_{4(S)} + O^{2-} - 2\,e^- \leftrightarrow 3\,Fe_2O_{3(S)}. \quad (6)$$

Finally, in air atmosphere at the high temperature conditions mainly of FeO (*wustite*) as chemical corrosion product exists on surface of stainless steel and joint. The mass rations of the oxides: $Fe_2O_3/Fe_3O_4/FeO$ are typically as 1/4/95%. Moreover, the stoichiometry of $Fe_yO$ is often approximated by y ~ 0.95, but the atomic ratio may range from 0.88 to 0.95. Oxidation is the formation of oxide rich scale. The scale, once formed, slows down further oxidation, unless it is mechanically removed or cracked which can happen if the material deforms under load.

The scale coat was replenished additionally as result of the oxidation of chrome:

$$4\,Cr + 3\,O_{2(g)} \rightarrow 2\,Cr_2O_{3\,(S)}. \quad (7)$$

and:

$$2\,Fe^{2+} + Cr_2O_{3(S)} + O^{2-} \leftrightarrow (Fe,Cr)_2O_{4(S)}. \quad (7a)$$

Moreover, on surface of metals were produced homogeneous of highly stable *spinel layer* of type of $(Fe,Cr)_2O_4$ (reaction (7a)), which is presented in Figure 6.

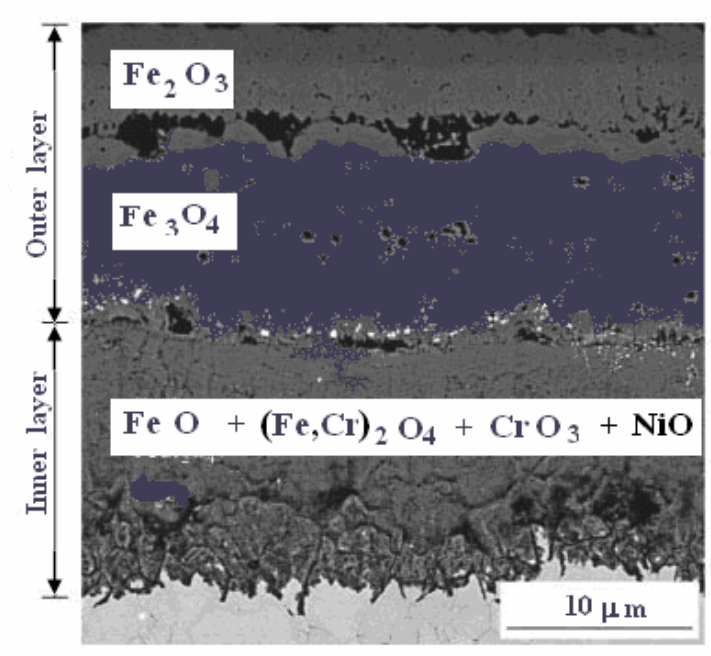


**Figure 6.** Scanning electron microscope images internally oxidized of join in air atmosphere for 90 minutes at temperature of 1200 $^0$C

The spinel layers protect effectively of metals surface layer before more far oxidation [25]. Unfortunately, the spinel layers break up / transformation at the high temperature (higher than 1400 $^0$C) and oxidation or chemical corrosion of substrates progress very quickly. The $Cr_2O_3$ surface layer is not durable, and after crossing temperature about 950 $^0$C get start next oxidation reaction:

$$2\ Cr_2O_{3(S)} + 6\ O^{2-} \rightarrow 4\ CrO_{3(S)}. \quad (8)$$

The $CrO_3$ is mobile in nature and diffuse to interior (Fig. 6) oxides scale.

Nickel also helps improve oxidation resistance of stainless steels and joint. This probably due to improved oxide layer adhesion.

The outer oxides scale on surface of metals were replenished by nickel oxide which creates according reaction:

$$2\ Ni + O_2 \rightarrow 2\ NiO_{(S)}. \quad (9)$$

However, the compositions of scales for multiple alloys are usually varied (see Fig. 6). In the case of TP347HFG and VM12-SHC stainless steels the compiled composition concerns the scale of the joint because it contains mainly: of iron, chrome and nickel oxides. Moreover, the scale does not protect the material prior to chemical corrosion at the high temperature conditions [25]. Figure 7 shows the images of the TP347HFG, joint and VM12-SHC stainless steels after thermogravimetric measurements.

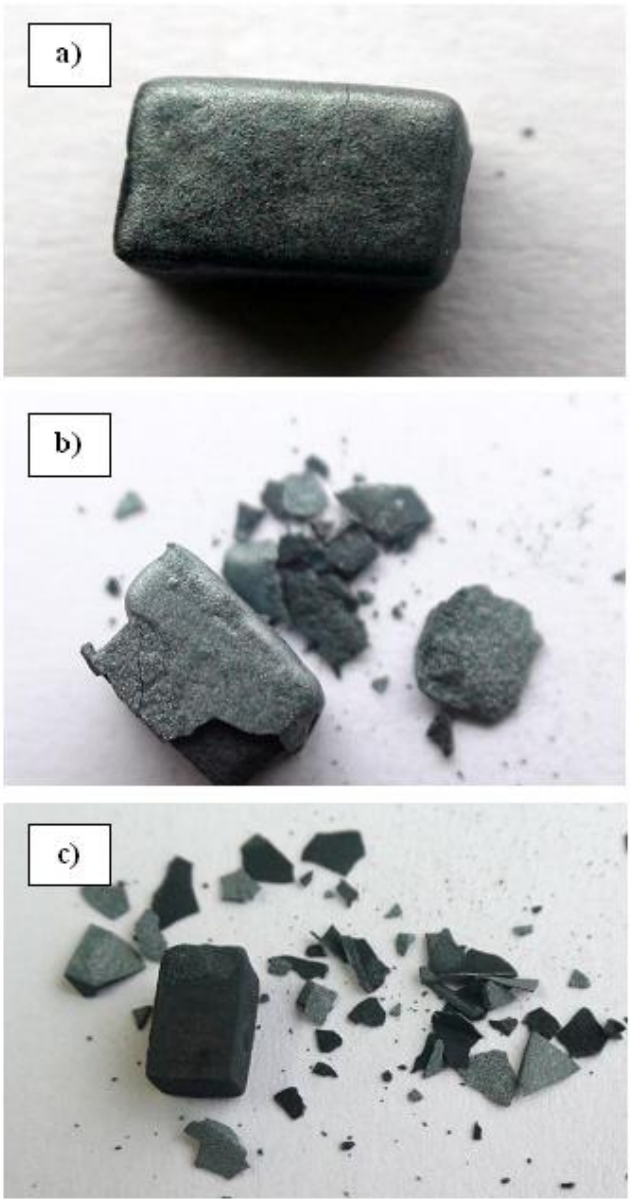


**Figure 7.** Images stainless steels and joint after thermogravimetric measurement: a) TP347HFG, b) joint and c) VM12-SHC

It can be seen that on the surface of TP347HFG the compact uniform and hard oxide layer was formed which protects the steel prior to high-temperature corrosion. However, in the case of VM12-SHC and the joint, due to the dissociation pressure the top oxide layer undergoes cracking on small pieces exposing the deeper layers of materials.

### *3.3. Ellingham diagram*

The Ellingham diagram is essentially a graph representing the thermodynamic driving force for a particular reaction to occur, across a range of temperatures. The diagram plots represent the standard free energy change ($\Delta G^0$) of a reaction as a function of temperature.

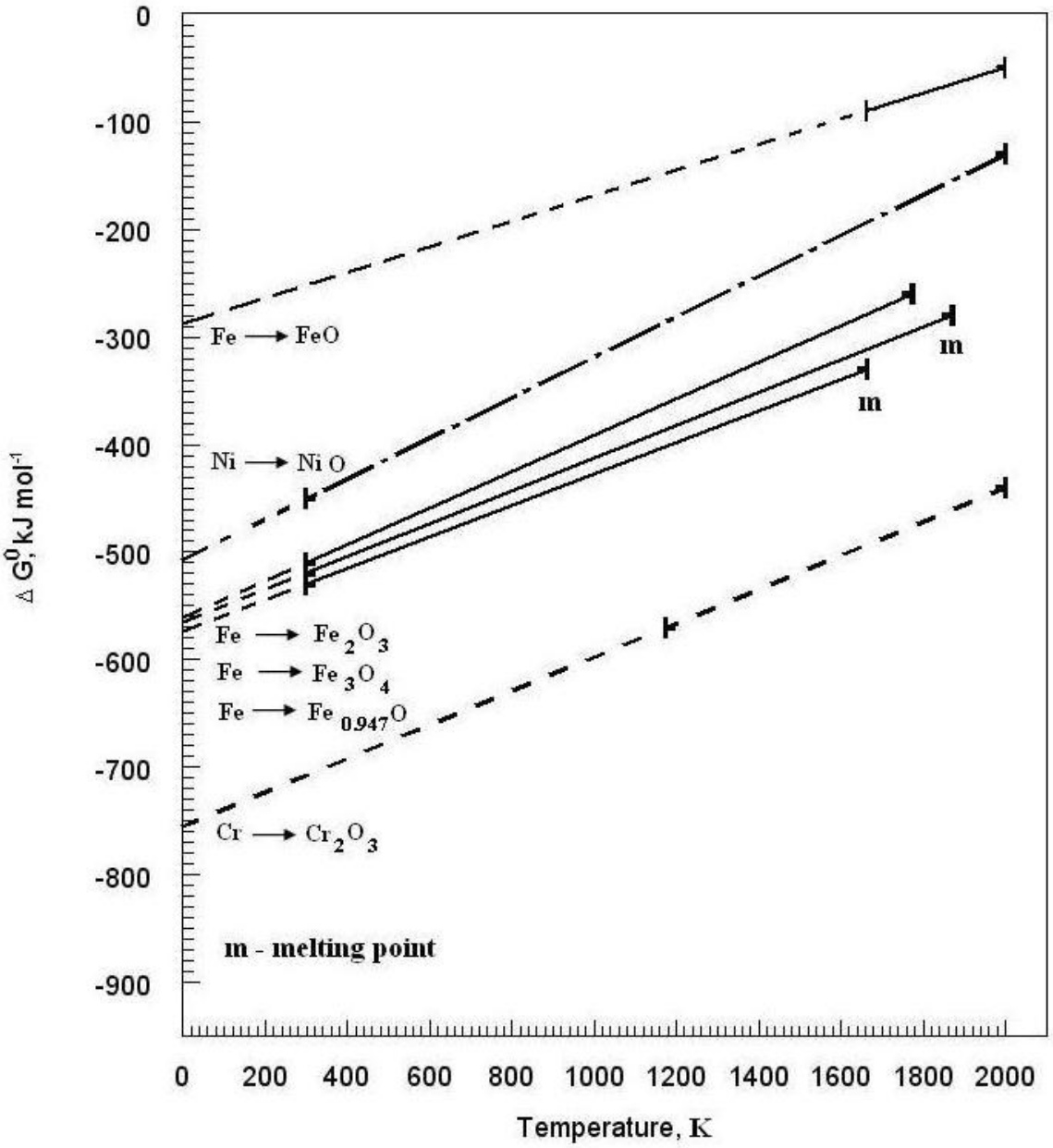


**Figure 8.** Ellingham diagram for reactions formation of oxides of iron, chrome and nickel

The free energy change of a chemical reaction is the difference in free energy between the products of the reaction and the reactants. A chemical reaction will occur if the total free energy of the products is less than total free energy of the reactants. If the system coating the reactants and products is closed the concentration of reactants will decrease and the concentration of products will increase as the reaction proceeds [26]. Figure 8 shows the Ellingham diagram for formation oxides of iron, chrome and nickel ($\Delta G^0 = - RT \ln p\ O_2$). A negative values for $\Delta G^0$ show that formation oxides of Fe, Cr and Ni are proceed spontaneously without external inputs. The standard free energy change is greater (more negative) for the chrome reaction relative to that of iron and nickel at all temperatures. This means that at all temperatures the equilibrium constant is larger for the chrome reaction, therefore the composition is further weighted towards the products of the reaction. This is the reason that metals that

appear higher up on the diagram (Ni) are more stable than those metals that appear lower down (Cr, Fe) and are more likely to be found in their pure oxides solid form. Moreover, the free energy change for chrome oxidation reaction is much lower than for iron oxidation reaction, that means that Cr is more oxidative than Fe. By using the diagram (Fig. 8) the standard free energy change for reactions formation of oxides of Fe, Cr and Ni can be found at 1200 $^0$C. The values of equilibrium constant and $\Delta G^0$ were listed in Table 3.

**Table 3.** Reaction formation of oxides, equilibrium constants, and standard free energy change at 1200 $^0$C

| **Reaction** | **Equilibrium constant** | **$\Delta G^0$ kJ / mol** |
|---|---|---|
| Ni → NiO | $5.26 \times 10^7$ | -218 |
| Fe → $Fe_2O_3$ | $3.31 \times 10^{10}$ | -296 |
| Fe → $Fe_3O_4$ | $2.97 \times 10^{11}$ | -323 |
| Fe → $Fe_{0.947}O$ | $1.06 \times 10^{12}$ | -339 |
| Cr → $Cr_2O_3$ | $4.34 \times 10^{17}$ | -497 |

Therefore, the Ellingham diagram was often used in extraction metallurgy to find the conditions needed for reduction of metal ores.

### *3.4. Oxidation rate*

Oxidation of material can be defined as the formation of a dispersed metal oxide near to the surface of an alloy. This layer consists of very fine metal oxide particles composed of one or more alloy elements. The oxidation (or chemical corrosion) rate of samples were calculated on basis Equation (1). The results are shown in Figure 9.

The kinetics of TP347HFG, joint and VM12-SHC stainless steels in the atmosphere of air were studied by fitting the corrosion data into different rate laws. Even through kinetic data may be interpreted as parabolic, the straight line is the easy fit [27,28]. As a result linear correlation coefficients ($R^2$) were used to determine the best law for the corrosion process. The rate laws were listed in Table 4. The obtained plots were linear with good correlation coefficient ($R^2 > 0.98$) confirmed that the corrosion of materials follows zero order kinetics. It can be observed that the rate constant oxidation reaction for joint achieves average value in comparison to both steels (see Table 4). However, joint was created as result good mixing components of TP347HFG and VM12-SHC stainless steels.

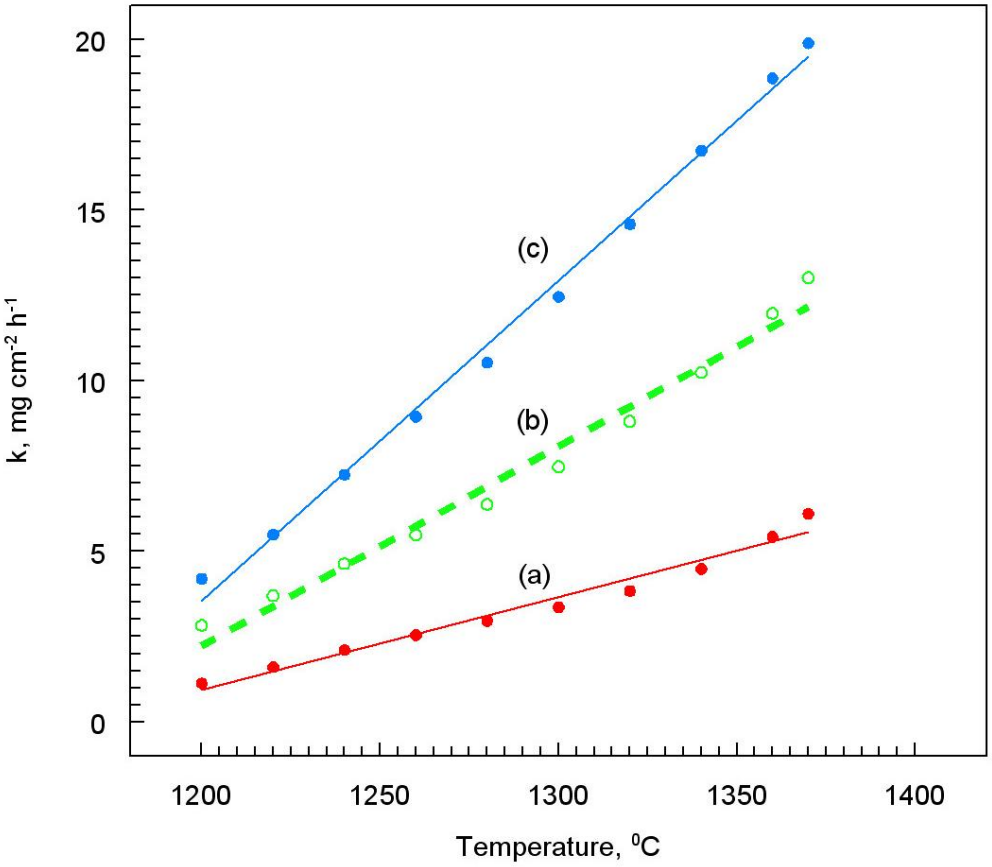


**Figure 9.** Oxidation rate as function of temperature for stainless steels and joint: (a) TP347HFG, (b) joint and (c) VM12-SHC. Heating rate of 5 $^0$C min$^{-1}$

**Table 4.** Materials, linear correlation coefficients and rate laws

| **Material** | $R^2$ | **Rate law** (for curves (a) – (c)) |
|---|---|---|
| TP347HFG | 0.9977 | $k_c = 0.094\,t - 108.9$ |
| Joint | 0.9897 | $k_b = 0.058\,t - 68.0$ |
| VM12-SHC | 0.9854 | $k_a = 0.027\,t - 31.6$ |

The evolution of the corrosion rate of substrates is directly attributed to the nature of corrosion products. The clear increase of the corrosion rate of materials can be observed at the high temperature of air atmosphere.

This can be explained by the by the replacement of the protective spinel film by non-protective porous films of oxide layers, which are then responsible for increasing the corrosion rate suitably to increase of temperature of TP347HFG, joint and VM12-SHC stainless steels.

### *3.5. Activation energy*

Activation energy ($E_a$) may be defined as the minimum energy required to start a chemical reaction. Moreover, $E_a$ can be thought as the height of the energy barrier separating two minima of potential energy of the reactants and products of a reaction.

According to Equations (2) or (2a) a plot of ln $k$ against 1/$T$ should be a straight line. Figure 10 presents the Arrhenius plots for the joint and both stainless steels. The linear correlation coefficients ($R^2$ > 0.98) were good for linear plots. Therefore, the slope of the line can be used to estimate the activation energy ($E_a$) of the oxidation process of materials. However, the linear correlation coefficients and the activations energy are given in Table 5. The value of activation energy for joint in the atmosphere of air is suitably high because it averages of 173.6 kJ/mol.

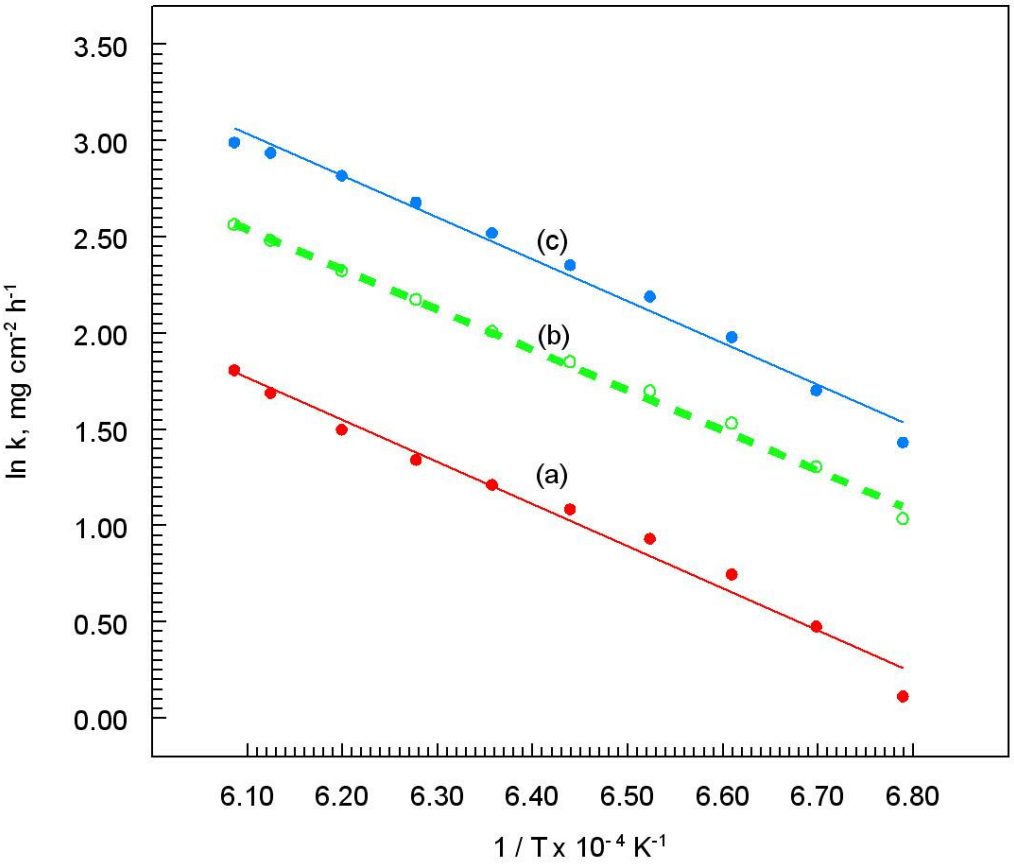


**Figure 10.** Arrhenius plots of ln $k$ versus 1 / $T$ for stainless steels and joint: (a) TP347HFG, (b) joint and (c) VM12-SHC

**Table 5.** Materials, linear correlation coefficients and activations energy

| Material | $R^2$ | $E_a$ kJ / mol |
|---|---|---|
| TP347HFG | 0.9977 | 182.1 |
| Joint | 0.9897 | 173.6 |
| VM12-SHC | 0.9854 | 170.3 |

This results confirmed the earlier advanced presumption that on result melting of TP347HFG and VM12-SHC stainless steel ally creates as joint which in air atmosphere and high temperature resistantly it oxides.

*3.6. Microhardness profiles and microstructures*

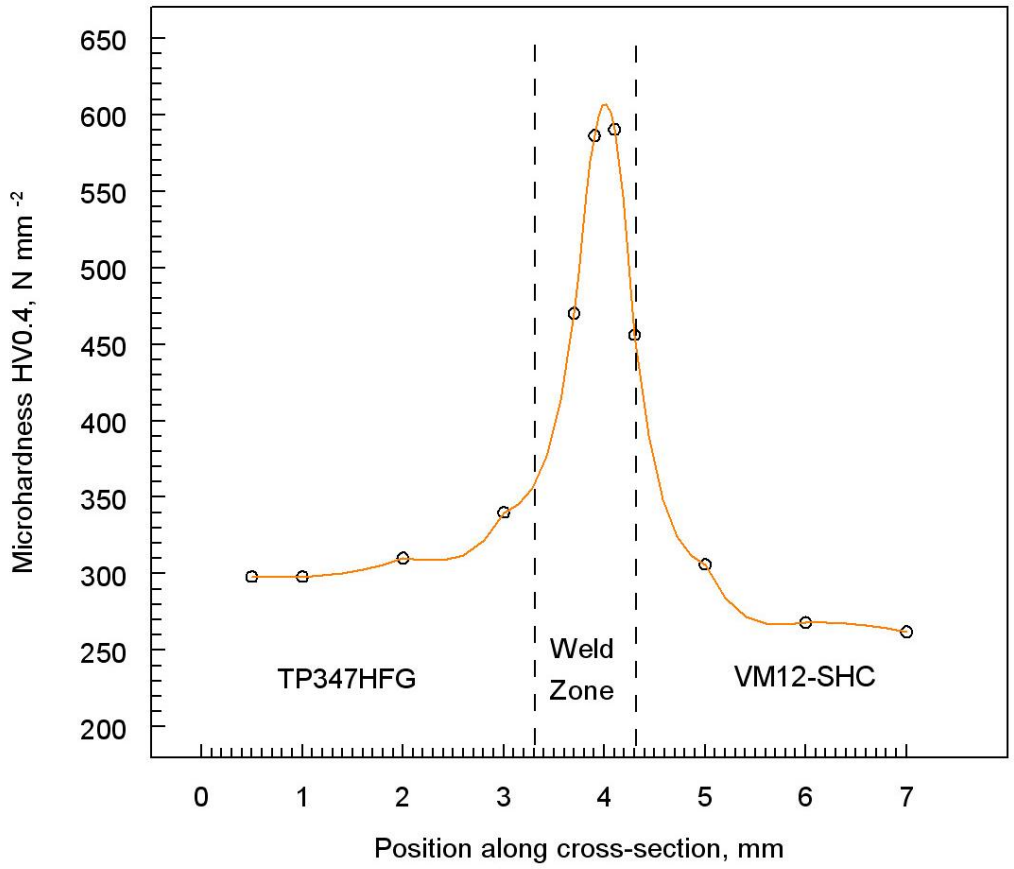


**Figure 11.** Vickers microhardness profile along the cross-section in specimens

The microhardness profiles of the specimen were analyzed using the Vickers method. The results are presented in Figure 11. In the heat-affected zone an increase in microhardness of both steels was observed. The maximum hardness value is located in the weld zone (about 580 HV0.4). The hardness of the joint increased about twice as much in comparison to the hardness of steels. The HV value indicates that the joint is fragile, and has low strength on hitting in relation to stainless steels. In this case special heat treatment should be applied after laser welding.

The scanning electron microscope images of the microstructure of the samples are shown in Figure 12.

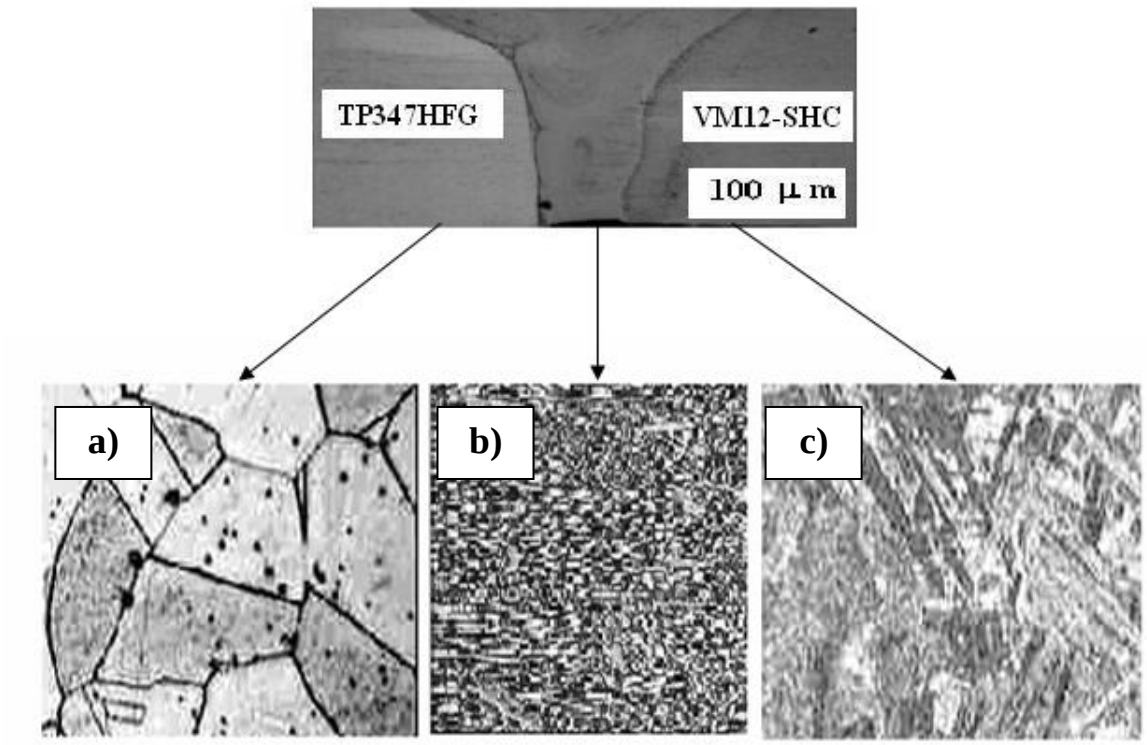


**Figure 12.** Scanning electron microscope images of microstructure: a) TP347HFG, b) joint and c) VM12-SHC stainless steel. Magnification 1000×

The characteristic austenitic microstructure (Fig. 12a) was observed for TP347HFG as well as the martensitic microstructure (Fig. 12c) for VM12-SHC stainless steel. Moreover, observations revealed a fine grained microstructure, and basically dendritic in the weld zone (Fig. 12b). The material which possesses dendrite microstructure is usually very hard. However, this type of microstructure is a result of high cooling rates typical of the laser welding process.

## 4. CONCLUSIONS

Considering the overall experimental results, the following conclusions can be drawn:

(1) The $CO_2$ laser welding is a good technique for joining dissimilar materials i.e. TP347HFG and VM12-SHC stainless steels.

(2) The chemical composition of the joint after $CO_2$ laser welding was different in comparison to both steels.

(3) The thermogravimetric data indicate that in air atmosphere and at the high temperature conditions the stainless steels and joint undergo oxidation / chemical corrosion.

(4) The joint has the medium resistance to oxidation in relation to both steels.

(5) The weld zone revealed a fine microstructure and was basically dendritic, due to the high cooling rate which is characteristic of the laser welding process.

(6) The values of Vickers microhardness indicates that the joint is fragile, and has low strength on hitting in relation to both stainless steels.

ACKNOWLEDGEMENT

This research was supported by *The National Centre of Research and Development*, a project of Technologies of Laser Welding for Energetic and the Protection of Environment (No. PBS1/B5/13/2012). The research part of the project of *1.3. Investigation of corrosive resistance of joints in the high-temperature conditions* was realized in the Institute of Chemistry, Jan Kochanowski University in Kielce.

**References**

1. L. Zhang, G. Fontana, *J. Mater. Process Technol.*, 74 (1998) 174
2. S. Katayama, *Weld Inter.*, 18 (2004) 618
3. A.P. Mackwood, R.C. Crafer, *Opt. Laser Technol*., 37 (2005) 99
4. C.T. Kwok, K.H. Lo, W.K. Chan, F.T. Cheng, H.C. Man, *Corros. Sci.*, 53 (2011) 1581
5. S.H. Baghjari, S.A.A. AkbariMousavi, *Mater. Des*., 57 (2014) 128
6. A. NaseryIsfahany, H. Saghafian, G. Borhani, *J. Alloys Comp*., 509 (2011) 3931
7. J.C. Lippold, D.J.Kotecki, *Ed. John Wiley & Sons*, NJ, USA, (2005)
8. C. Weichiat, A. Paul, M. Pal, *Mater. Des*., 30 (2009) 245
9. L.C. Chan, S.M. Chan, C.H. Cheng, T.C. Lee, *J. Eng. Mater. Technol.*, 127 (2005) 179
10. H. Lee, H.S. Hamb, *Mater. Sci. Eng. A.*, 415 (2006) 149
11. C.H. Cheng, L.C. Chan, C.P. Lai, C.L. Chow, *J. Mater. Manuf.*, 01-0353 (2006) 327
12. L. Fratini, G. Buffa, R. Shivpuri, *Mater. Sci. Eng*., 459 (2007) 209
13. M. Scendo, J. Trela, B. Antoszewski, T. Kargul, *Innovat. Corros. Mater. Sci*., 4 (2014) 1
14. M. Otero, M.E. Sanchez, X. Gòmez, A. Morán, *Waste Manage.*, 30 (2010) 1183
15. M. Varol, A.T. Atimaty, B. Bay, H. Olgum, *Tchermochim. Acta*, 510 (2010) 195
16. C.X. Chen, X.Q. Ma, K. Liu, *Appl. Energy*, 88 (2011) 3189
17. A.A. Zuru, S.M. Dangoggo, U.A. Birnin-Yauri, A.D. Tambuwal, *Renew. Energy*, 29 (2004) 97
18. H.M. Xiao, X.Q. Ma, Z.Y. Li, *Appl. Energy*, 86 (2009) 1741
19. M. Bouklah, A. Attayibat, S. Kertit, A. Ramdani, B. Hammouti, *Appl. Surf. Sci.*, 242 (2005) 399
20. M. Bouklah, B. Hammouti, M. Lagrenée, F. Bentiss, *Corros. Sci*., 48 (2006) 2831
21. M. Scendo, *Corros. Sci*.,47 (2005) 1738
22. M. Scendo, *Corros. Sci*.47 (2005) 2778
23. M. Scendo, J. Trela, N. Radek, *Corros. Rev*., 30 (2012) 33
24. M. Danielewski, *Sol. State Ion.*, 45 (1991) 245
25. I.G. Crouch, J.C.Scully, *Oxidat. Met.*, 15 (1981) 121

26. Atkins Peter, de Paula Julio. *Physical Chemistry: Thermodynamics and Kinetics* (8th ed.), W.H. Freeman (2006)
27. M.K. Pavithra, T.V. Venkatesha, M.K. Punith Kumar, H.C. Tondan, *Corros. Sci.*, 60 (2012) 104
28. M. Scendo, J. Trela, *Int. J. Electrochem. Sci.*, 8 (2013) 8329